Journal of Innovative Materials in Extreme Conditions
2020
Volume 1
Issue 1

METAL-LIKE THERMAL CONDUCTIVITY POSSESSED BY ATMOSPHERE ASSISTED SYNTHESIS OF SPARK PLASMA SINTERED MAYENITE ($Ca_{12}Al_{14}O_{33}$)

Teslin Johnson[1], Eranezhuth Wasan Awin[1], Marija Prekajski Djordjevic[2], Branko Matovic[2], Ravi Kumar[1, *]

[1] Laboratory for High-Performance Ceramics, Department of Metallurgical and Materials Engineering, Indian Institute of Technology-Madras (IIT Madras), Chennai 600036, India
[2] Centre of Excellence "CextremeLab", Centre for synthesis, processing, and characterization of materials for application in the extreme conditions, Belgrade, Serbia
Corresponding author: nvrk@iitm.ac.in*

Abstract: *Mayenite ($Ca_{12}Al_{14}O_{33}$) samples have been synthesized in ambient air, argon, and nitrogen atmospheres to vary the defect chemistry and to investigate its role in thermal conductivity. Highly dense sintered pellets (SEM) were obtained through spark plasma sintering and the X-ray diffractograms revealed predominantly mayenite phase with the presence of a minor amount of secondary phases. Thermal conductivity was measured for the sintered samples and it was observed that mayenite synthesized in nitrogen atmosphere exhibited a colossal value of 579 $Wm^{-1}K^{-1}$ at room temperature close to that of cubic-BN, comparable with that of metals.*

Keywords**:** *ceramics, sintering, transport properties, thermal conductivity.*

1. Introduction

The calcium aluminate based compound, *mayenite* has attracted intense interest due to its highly tunable electrical and optical properties resulting in applications such as solar cells, flat panel displays, organic light-emitting devices, and gas sensing devices [1]. Mayenite has the ability to incorporate many anions such as Cl^{-1}, OH^{-1}, and even electrons in its cage structure [2].

Mayenite exhibits different physical properties depending on the replacement of free "oxygen" with anions (F^-, Cl^-, OH^-, O_2^- and H^-)/cations (Ga, Sr, Al, Zn, Fe, and Cu) in the nano-cages without much change in the lattice structure [3, 4]. The caged oxygen ions can be gradually replaced with electrons generating a series of compounds with the formulae; $[Ca_{12}Al_{14}O_{32}]^{2+}\,O^{2-}_{1-\delta}\,e^-_{2\delta}$ ($0 \leq \delta \leq 1$) making these materials insulating at $\delta = 0$ and metallic conducting electrides at $\delta = 1$, where electrons form ionic bonds with the framework [5-6]. Recently, it was also shown that doping of mayenite with Sn and Si resulted in high conductivity values of 280 $S.cm^{-1}$ and 300 $S{\cdot}cm^{-1}$ respectively [7]. The removal of loosely bound "free oxygen" by ions plays a crucial role in determining the thermal properties as well. However, limited reports are available toward understanding the thermal properties of mayenite.

The heat conductivity in a material is contributed by both phonons (lattice conductivity) and free electrons (electron conductivity) and are related by the Wiedemann-Franz law; $K \alpha \sigma T$. Hence, by varying the defect chemistry of mayenite, it is believed that the electronic contribution to the heat conductivity in mayenite could be altered. Kim et al. reported thermal conductivity values in the range 2.3 - 4.5 $Wm^{-1}K^{-1}$ at 300 K, exhibiting an amorphous type T^2 dependency at lower temperatures in single crystals of mayenite [8]. Recently, the presence of O_2^- ion vacancies were found to reduce the thermal conductivity of the spark plasma sintered mayenite/nano-carbon black composites [9]. The activated bamboo charcoal/C12A7 mayenite composites reported lower thermal conductivity values ranging between 1.2 - 1.4 $W\,m^{-1}K^{-1}$ at room temperature due to carbon diffusion [10].

In this work, we try to realize the effect of processing atmospheres on the thermal properties of dense mayenite samples. The polycrystalline mayenite samples were synthesized in controlled atmospheres (air, argon, and nitrogen) and were subjected to spark plasma sintering to obtain dense pellets. Herein, we report for the first time the colossal thermal conductivity values for mayenite samples prepared in air and nitrogen atmospheres.

2. Results and discussion

The X-ray diffractograms of both powder samples and pellets showed the presence of crystalline mayenite with a minor fraction of secondary phases such as calcium dialuminate and tricalcium dialuminate as shown in Figure 1(a) and (b). These phases occur on both sides of the line compound mayenite in the $CaO\text{-}Al_2O_3$ phase diagram and were inevitable. The lattice parameters calculated from the powder X-ray diffractograms of M/air, M/N_2, and M/Ar are tabulated in Table S1. The cell volume of M/N_2 is 1.08% larger than that of M/air and M/Ar is 1.23% larger than that of M/air.

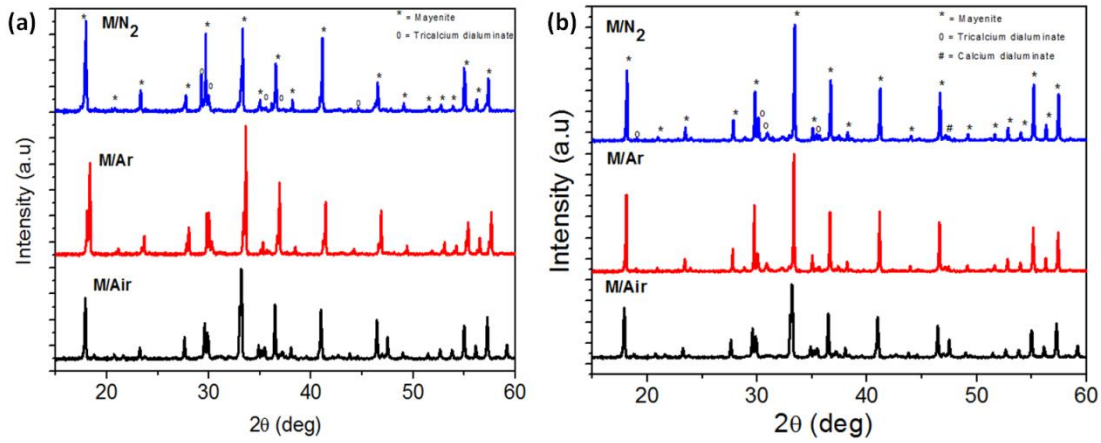

Figure 1. X-ray diffractograms of M/air, M/N_2, and M/Ar **(a)** powder and **(b)** spark plasma sintered pellet revealing the presence of phase pure mayenite.

The increase in cell volume could be attributed to the extra framework of oxygen ions that gets replaced with electrons. As a result of this, the cage structure of mayenite is expected to relax due to the weak interaction of the framework with the electrons, which is in line with earlier observations [11]. Hence, we hypothesize that the lattice parameter increase from M/air to M/N_2 and M/Ar (Table. S1) is due to the electron replacement with oxygen ions. The density of the sintered mayenite pellets has been tabulated in Table. S2. Near true densities have been obtained for all three samples. The true density decreases from that of pure mayenite with higher electron loading and this could be observed in the reduction in density from M/air to M/N_2 and M/Ar.

The mayenite exhibits several modes in the range of 100-1500 cm^{-1} in its Raman spectra which are assigned to the Al-O vibrations in the framework (Figure 2). The most prominent mode at 520 cm^{-1} is ascribed to the Al-O-Al vibration of the bridge oxygen in the AlO_4 tetrahedrons. The Al-O stretching vibrations within AlO_4 tetrahedrons give rise to the modes at 771 cm^{-1}, 881 $cm^{-1,}$ and 916 cm^{-1} [12]. Doubly and triply degenerated framework oxygen atoms contribute to the group of weaker modes between 150 cm^{-1} and 400 cm^{-1} in the spectra [13-15].

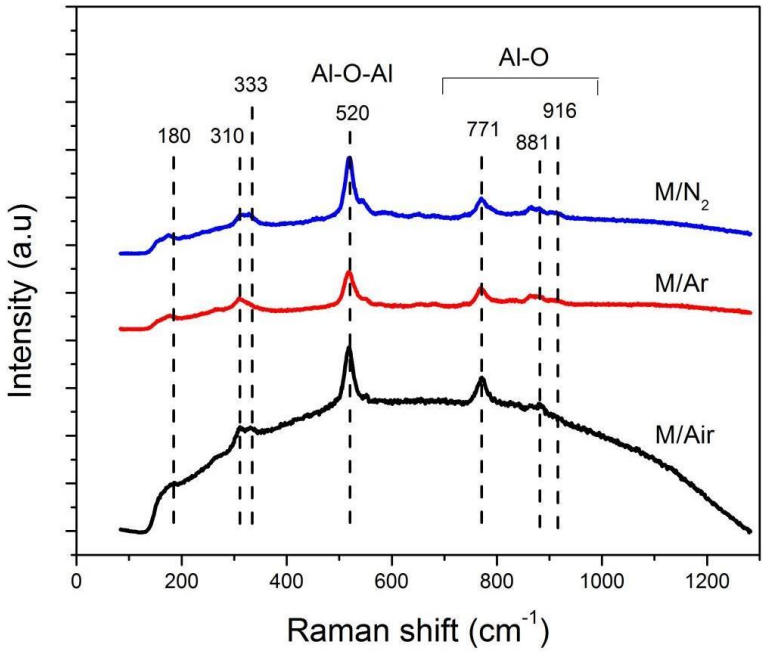

Figure 2. Raman spectra of the pellets of M/air, M/N_2, and M/Ar confirming the presence of mayenite.

The SEM micrographs as exemplified in Figure 3a clearly show the microstructures of the sintered sample with grain size varying in the range of 400-500 nm and trigeminal grain boundaries. The grains were densely sintered, pore, and crack-free with the absence of secondary phases at the grain boundaries. The microstructures appeared to be defect-free at the nanoscale regime.

The thermal diffusivity (α) values vary significantly between the three samples as shown in Table 1.

Table 1. Thermal diffusivity values obtained by laser flash technique

Temperature (℃)	α-M/air (x 10^{-4} m^2/s)	α-M/N_2 (x 10^{-4} m^2/s)	α-M/Ar (x 10^{-4} m^2/s)
35	1.395	2.397	0.0116
199	---	2.179	0.0084
404	---	2.133	0.0066
606	1.213	2.062	0.0058
799	1.019	1.753	---

The α values of M/N_2 are almost double that of M/air at all temperatures and the α of M/Ar is almost 2 orders less than that of M/air and M/N_2. The α values were found to be decreasing with an increase in temperature and could be attributed to the increase in phonon and electron scattering at higher temperatures. The C_p values were observed to increase parabolically with respect to temperature as given in Figure 3b. The C_p values increased with an increase in temperature as vibrational and rotational degrees of freedom become increasingly dominant in the total enthalpy of the system. The k values in turn obtained as the product of thermal diffusivity, density, and specific heat capacity as a function of temperature are shown in Figure 3c.

It could be noted that the k value of M/N_2 is anomalously high (~ 579 W/m.K at 600 °C) comparable to that of metallic thermal conductors such as silver, copper, and other metals and close to high thermally conducting ceramics such as cubic boron nitride. The k values of M/Ar were in the order of 1.5-3.0 W/mK which was in accordance with the values reported by Sung Wng Kim [16]. However, the reasons behind the anomalously high values of thermal conductivity of M/N_2 and M/air

are still not clear. We believe that the processing atmosphere (air and nitrogen) could have altered the defect chemistry resulting in colossal thermal conductivity values.

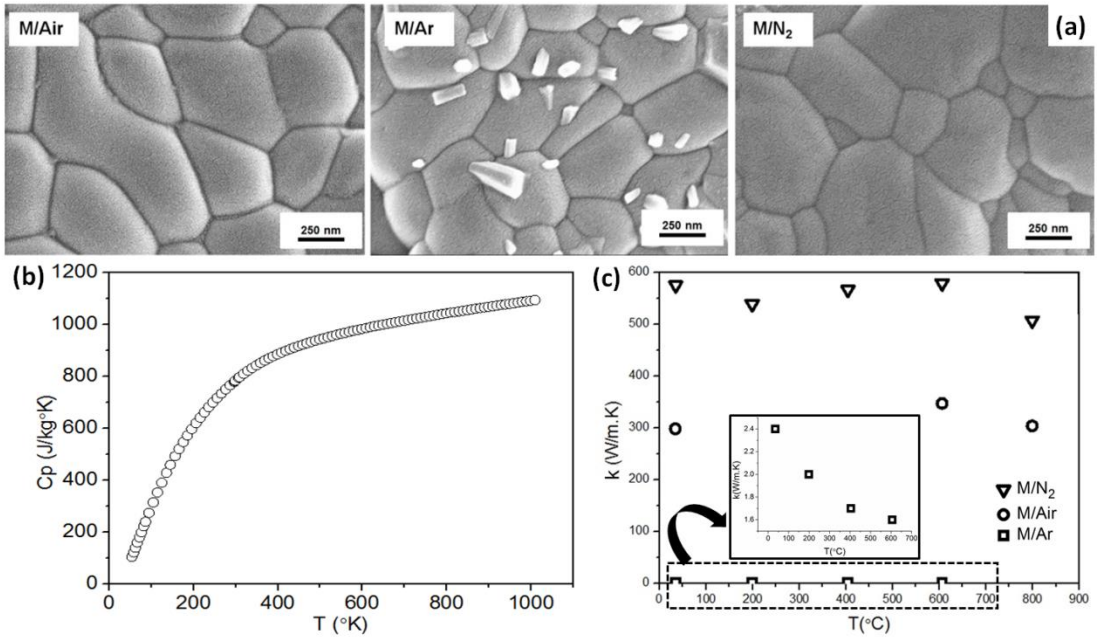

Figure 3. (a) SEM micrographs of the pellets of M/Air, M/Ar, and M/N_2 **(b)** Specific heat capacity (C_p) of mayenite as a function of temperature (T) [28-29] and **(c)** Thermal conductivity of M/air, M/N_2, and M/Ar. The inset image shows the magnified view of k (M/Ar) vs T

3. Conclusion

The transport properties of spark plasma sintered mayenite samples synthesized in controlled atmospheres (air, nitrogen, and argon) have been investigated. The XRD and Raman spectroscopy confirmed the formation of the mayenite phase with a small amount of secondary phases. The transport properties were found to be significantly influenced by the processing atmosphere. The high thermal conductivity value of M/N_2 (k > 500 W/mK) is comparable to that of metals and is expected to be due to the alteration in defect chemistry as a result of varying processing atmospheres. However, the transport mechanisms have to be still elucidated.

References

1. M. M. Rashad, A. G. Mostaf, and D. A. Rayan., Middle East J. Appl. Sci., 2015, 5, 79-86
2. G. Hentschel, Neues Jahrb. Mineral. Monatshefte, 1964, 22–29
3. Elnaz Feizi et.al, Journal of display technology, Vol.12, No.5 (2016)
4. J. Huang, L. Valenzano and G. Sant, Chem. Mater, 2015, 27, 4731−4741.
5. W. Zhou, W. Yu, Y. Li and S. Tang, Mater. Lett., 2019, 251, 106–109.
6. F. Li, X. Zhang and H. Liu J Am Ceram Soc., 2020, 103, 35–42.
7. K. Khan, A. khan Tareen, U. Khan, A. Nairan, S. Elshahat, N. Muhammad, M. Saeed, A. Yadav, L. Bibbò and Z. Ouyang, Sci. Rep. 2019, 9:4967
8. S. W. Kim, R. Tarumi, H. Iwasaki, H. Ohta, M. Hirano and H. Hosono, Phy. Rev. B, 2009, 80, 075201.
9. C. Rudradawong, M. Kitiwan, T. Goto, and C. Ruttanapun, Mater. Today Commun., 2020, 22, 100820.
10. C. Rudradawong and C. Ruttanapun, Mater. Chem. Phys., 2019, 226, 296–301.
11. L. Palacios, A. G. De La Torre, S. Bruque, J. L. Garcıa-Munoz, S. G. Granda, D. Sheptyakov, and M. A. G. Aranda, Inorg. Chem. 2007, 46, 4167−4176.
12. P. McMillan and B. Piriou, J. Non-Cryst. Solids, 1983, 55, 221–242,
13. K. Kajihara, S. Matsuishi, K. Hayashi, M. Hirano and H. Hosono, J. Phys. Chem. C, 2007, 111, 14855–14861.
14. M. Ruszak, S. Witkowski, P. Pietrzyk, A. Kotarba and Z. Sojka, Funct. Mater. Lett., 2011, 04, 183–186
15. Y. Yin, Z. Jia, W. Mu, Z. Gao, J. Zhang and X. Tao, Cryst. Growth Des., 2016, 16 (4), 1903–1906.
16. S. W. Kim, R. Tarumi, H. Iwasaki, H. Ohta, M. Hirano and H. Hosono, Phy. Rev. B., 2009, 80, 075201.